



Universiteit
Leiden
The Netherlands

Opleiding Informatica

Automated Analysis of Cardiomyocyte Maturation in
3D Organoids Under Multi-Axial Cyclic Preload

Marjolein van Tol

Supervisors:
Lu Cao

BACHELOR THESIS

Leiden Institute of Advanced Computer Science (LIACS)
www.liacs.leidenuniv.nl

20/01/2025

Abstract

This paper analyses the effect of multi-axial cyclic preload on cardiomyocyte maturation in mini-heart. Where the models are derived from human induced pluripotent stem cells (hiPSCs). We use existing high-throughput image analysis models to explore their efficacy in evaluating sarcomere and fibril structures. Results show that cyclic preload may enhance cardiomyocyte maturation, with key improvements observed in sarcomere structure and fibril length. The FFT and Fibril analysis methods show promising performances and highlight the potential for future research in optimizing imaging protocols and computational tools. This will result in better analysis and understanding of cardiomyocyte development.

Contents

1	Introduction	1
1.1	Cardiomyocytes	1
1.1.1	Sarcomeres and Z-disks	1
1.1.2	Cardiomyocytes maturation	1
1.2	Stimulating mini hearts	2
1.2.1	Mini hearts	2
1.2.2	3D culturing conditions	2
1.3	Automatic image analysis	2
1.4	Research questions	3
1.5	Overview	3
2	Definitions	3
3	Related Work	4
3.1	High-throughput imaging	4
3.2	Material Gathering	4
3.2.1	Stretching mini-hearts	4
3.2.2	Labeling	5
3.2.3	Imaging	5
3.2.4	Z-line segmentation	7
4	Experiments	8
4.1	Fibril analysis	8
4.2	Sarcomere Analysis	10
4.2.1	BM tracing	10
4.2.2	FFT-2D	12
4.3	The tool	14
4.3.1	Parameters	14
4.4	Results	15
4.4.1	Fibril Analysis	15
4.4.2	Sarcomere Analysis	18
4.4.3	Runtime	19

5 Conclusions and Further Research	19
5.1 Fibril Maturation	20
5.2 Sarcomere Maturation	21
5.3 Research Conclusion	21
5.4 Further Research	22
References	25

1 Introduction

Heart failure is a significant global health concern, often caused by drug-induced cardiotoxicity [CSD⁺22]. Heart failure is the leading cause of hospitalization in the United States, and cases continue to grow as the population ages [PE09]. Due to a lack of reliable models, understanding the mechanisms behind this problem is quite difficult. A research group showed that nearly 90% of the benefits of perfect heart disease care come from interventions before and between heart attacks [KFJ⁺09], which also reduces the risk of death from other chronic diseases. This highlights the importance of quick diagnosis and prevention of heart damage. A paper from 2022 [CSD⁺22] suggested that human pluripotent stem cells (hPSCs) offer promise in modeling these types of diseases, mostly because of their ability to represent genetic variations.

1.1 Cardiomyocytes

The heart muscle is made up of cardiomyocytes. They are responsible for contracting the heart to generate the pressure needed to pump blood throughout the circulatory system. The heart forms early during embryonic development. In this period nearly all cardiomyocyte generation occurs [WM05]. After birth, most adult cardiomyocytes lose their ability to divide. During the postnatal phase, the heart grows not by generating new cells but through the enlargement of existing cells [WM05].

Although studies have shown that cardiomyocytes do renew throughout life, this occurs at an extremely slow rate. By the age of 25, only about 1% of cardiomyocytes regenerate annually, and this rate decreases with age [PE09]. The limited renewal and critical roles of these cells, make the loss or dysfunction of cardiomyocytes a leading cause to heart failure [PE09]. This underlines the significant impact of any damage to the heart.

1.1.1 Sarcomeres and Z-disks

The primary functional components of cardiomyocytes are myofibrils, which consist of repeating units called sarcomeres. Sarcomeres consist of thick and thin filaments organized into distinct bands. Z-discs, which are orthogonal to the sarcomere structure, play a critical role in stabilizing sarcomeres through interactions with α -actinin and other proteins. Mutations in Z-disc related proteins have been associated with cardiomyopathies [ATA22].

α -Actinin is used as a key marker for labeling muscle tissue during analysis. Its expression is controlled by the *ACTN1* gene, which can be tagged with fluorescent proteins to study Z-disc structures.

1.1.2 Cardiomyocytes maturation

Cardiomyocyte maturation can be defined by significant myofibril expansion and alignment [GP20]. This can be observed by analyzing the fibrils themselves and the sarcomere structure. Sarcomere maturation consists of structural improvements that make the organization of its components more efficient and precise [GP20]. Research has shown that during maturation, Z-disks become wider and better aligned, and the sarcomere length increases to approximately 2.2 micrometers in mature heart cells [GP20]. Moreover, some studies show that residual stress plays a critical role in the

biomechanics of tissues, creating more efficient structures [Tab01]. Research has demonstrated the positive impact of cyclic mechanical stress during induced cardiomyocyte maturation [MLM⁺14] [ATY⁺17] [TMR⁺11]. Key findings include a higher proportion and increased size of cardiomyocytes. Moreover, we also see improved myofibril and sarcomere structure and alignment, along with enhanced contractile elements.

1.2 Stimulating mini hearts

The university of twente is studying the effects of multi-axial cyclic preload on mini-heart functionality and cardiomyocyte maturation. By incorporating mechanical stimuli through cyclic stretch, they want to study whether this can favor overall mini-heart performance and cardiomyocyte maturation. Characterizing sarcomere length is a useful metric to assess this cardiomyocyte maturation.

1.2.1 Mini hearts

Mini hearts are fabricate engineered cardiac chambers using human induced pluripotent derived cardiomyocytes (hiPSC-CMs) and human cardiac fibroblasts (hcFBs) [CJKDASCT]. These chambers are hollow and coupled to a glass capillary that serves as an inlet to the lumen of the tissue. The mini-hearts are capable of pumping fluid when they contract. This is tracked by observing the displacement of liquid in the glass capillary.

hiPSC-CMs are characterized for being immature, resembling more a fetal heart rather than the adult heart. This immaturity can be reflected in different ways, one of them is the contractile performance which is linked to how developed sarcomeres are.

1.2.2 3D culturing conditions

The mini-hearts were initially created using 2D cell cultures, where cells are grown on a flat surface. More recently, 3D organoid cultures have been used, where cells grow in three-dimensional spaces. On a cellular level, a key difference is the way cells interact with each other and the culture medium, which is more dynamic in the 3D environment. A 2021 study found that while 2D cultures exhibited increased cell proliferation, they also showed altered cell polarity, suppressed signaling, and impaired neuron production [SAC⁺21]. In contrast, 3D organoids demonstrated more efficient signaling and enhanced neuron generation, closely mimicking the natural development process [SAC⁺21].

1.3 Automatic image analysis

In recent decades multiple biomedical imaging techniques have emerged [Pen08]. Ranging from advanced microscopy methods to improved labeling technologies. This has led to a rapid increase in digital biological images, with large and complex datasets. As a result, bioimage informatics has become a growing field, focused on developing algorithms and systems for analyzing and processing these images [Pen08].

Automated high-throughput analysis methods are used to help manage the vast amounts of data. Key techniques like feature extraction, segmentation, and classification enable efficient analysis of cellular behaviors and complex biological structures. Instead of manually analyzing each image, it significantly reduces the workload for research personnel. Recent advancements also show promising results with AI and deep learning methods, significantly improving clinical outcomes [PA20]. These

techniques are enhancing classification, segmentation, and image synthesis across various imaging methods.

1.4 Research questions

The University of Twente has multiple datasets of mini-hearts that they aim to study for functionality and cardiomyocyte maturation. The dataset consists of both stimulated and control conditions. Z-disk labeling and high-throughput image analysis are used to investigate cardiomyocyte features. Multiple algorithms have been developed for analyzing various aspects, such as fibril and sarcomere analysis. The samples were originally cultured under 2D conditions. Given the new experimental setup, we will adapt the existing models to suit these updated conditions. This leads us to the following research questions:

- How can we apply existing models to analyze 3D organoid cardiomyocytes derived from hiPSC-CMs?
- What are the effects of multi-axial cyclic preload on mini-heart cardiomyocyte maturation?

1.5 Overview

In this thesis, existing algorithms will be used to analyze mini-heart images to determine if stimulating the heart effects the maturation. In Section 1, an introduction is provided, explaining the context of the project and some key concepts needed for the report. In Section 2, the main definitions are presented. Next, in Section 3, related work is discussed, including a more in-depth overview of earlier algorithms, other studies conducted on this topic, and information about the heart samples. In Section 4, an in-depth view is given of the methodology of the experiment and the results that were obtained. Additionally, a tool is created to enable future experiments, which will also be discussed in this section. Lastly, Section 5 concludes the report with a discussion of the results and further research. Here, the main research question will also be answered.

In summary, this research will provide further insight into high-throughput imaging of stimulated mini-heart samples and introduce a tool to make these methods more accessible.

2 Definitions

For this research some terms will be referred to by their abbreviation. Firstly, the term human pluripotent stem cell derived cardiomyocytes will be referred to as hiPSC-CMs and cardiomyocytes sometimes as CMs. Next, three different methods will be used in this experiment. The fibril analysis which does calculations based on fibrils structure. The BM method refers to the binary mask of the image, which the method uses as input for the algorithm. Finally the FFT or 2D-FFT method which stands for the fourier frequency transform (FFT).

3 Related Work

A research group at the University of Twente has already demonstrated promising results for stimulating mini-hearts. Visual evidence indicates that dynamic preload conditioning improves mini-heart pump performance [CJKA^{SCT}]. Stimulated samples showed shorter cycle durations and faster relaxation times, which are key indicators of enhanced relaxation dynamics and more efficient calcium intake. These findings also suggest improved cardiomyocyte maturation.

3.1 High-throughput imaging

Previous work in automated high-throughput imaging has shown promising results. Research at Leiden University LIACS [CSD⁺22] demonstrated significant advancements in high-throughput image analysis of sarcomere structures in hiPSC-CMs. Further studies utilized high-throughput screening to evaluate the cardiotoxicity of 1,138 chemicals from the Tox21 library, successfully identifying 40 CV-relevant targets [KBK20]. In addition, new methods such as combining this approach with deep learning have supported early-stage drug discovery by identifying cardiotoxic risks [GHR⁺21].

3.2 Material Gathering

The samples were developed by the University of Twente, with additional information and contact provided by PhD candidate Mariel Cano-Jorge [CJKA^{SCT}].

In their research, they utilized ventricular filling with blood to impose a dynamic stretch (preload) on the myocardium. This process activates mechano-regulatory responses that contribute to cardiomyocyte maturation and the progression of cardiomyopathies. Engineered 3D cardiac tissues are often used to model heart diseases in the lab but are usually tested under static conditions. Adding dynamic preload (varying forces) to these models is challenging, requiring complex setups that can interfere with measuring tissue contractility. In contrast, engineered ventricles mimic the heart's pumping function.

With this, they established a mechanical stimulation protocol to replicate preload dynamics in human-engineered ventricles [CJKA^{SCT}]. The complete protocol will be discussed in the following section.

3.2.1 Stretching mini-hearts

First, stem cells are differentiated by cardiomyocytes (which are next frozen). For the experiment, the control and stimulated group are created from the same batch of differentiated CMs to avoid additional sources of variability.

Mini-hearts were created using a 3D-printed bioreactor. A gelatin mold is formed to shape the mini-heart, which is then filled by seeding hiPSC-CMs and human cardiac fibroblasts. When the gelatin molds degrade due to heat after fibril crosslinking, they form a hollow tissue structure that can be perfused through a glass capillary inlet. The mini-heart is surrounded by culture medium both internally and externally.

A syringe pump is connected to the capillary inlet via tubing, allowing fluid to be pumped in and

out over time to expand and contract the volume. This process applies 5% strain at 0.5 Hz for 4 hours a day. The glass capillary inlet provides volume data, and the displacement of liquid during beating cycles is used to estimate stroke volumes.

3.2.2 Labeling

First, the mini-hearts were fixed in 4% paraformaldehyde in PBS for 45 min at room temperature. This preserves the tissue morphology and cellular structures by stabilizing proteins and nucleic acids. The tissues were washed three times in PBS, removing any residual paraformaldehyde. Next, the sample is permeated with 0.3% Triton-X 100 (Sigma-Aldrich) for 20 min to permeabilize the cell membrane. This allows antibodies and other reagents to penetrate the cells. The tissues are then blocked in 3% BSA, 0.3% Triton-X 100, and 0.1% Tween in PBS overnight at 4 °C, this is used to block non-specific sites. Next, the tissues were incubated for 2 days at 4 °C with primary antibody anti-alpha-actinin (1:400; Invitrogen, MA5-12960). Here the antibody specifically binds to alpha-actinin. Incubating for 2 days ensures strong binding between the antibody and its target. The samples are washed three times in 0.3% Triton-X 100 for 20 minutes each time, to remove unbound antibodies. The tissues were then incubated with a secondary antibody (Goat-anti-Mouse IgG Alexa Fluor 647) at a dilution of 1:500 and DAPI for 24 hours at 4°C. The secondary antibody binds to the primary antibody (which was raised in a different species), enabling the detection of the primary antibody's location via fluorescence. Samples were then again washed three times in PBS, and mounted on a glass-bottom plate (Ibidi 81158) for the imaging.

For each mini heart there is a control (non-simulated heart) sample that was created from the same batch of differentiated CMs. They underwent the same staining, however did not undergo the multi-axial cyclic preload.

3.2.3 Imaging

Confocal microscopy is widely used as a specialized form of standard fluorescence microscopy. It is capable of producing high-resolution images of fluorescently stained samples. It offers significant advantages over traditional widefield fluorescence microscopy by eliminating out-of-focus light. This results in sharper and higher-resolution images [Pet10].

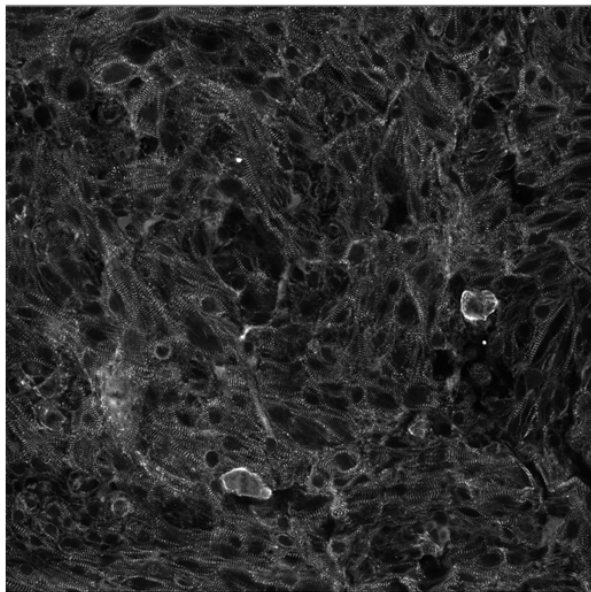
The imaging was performed using a Zeiss LSM 880 confocal microscope [mic]. Since the samples were three-dimensional, they had to be placed between two pieces of glass. To enhance imaging quality, a slight force was applied to flatten the samples.

For each mini-heart, nine images were captured in the orientation shown in image 1 and saved as TIFF files with one channel in 16-bit format. This thesis includes data from four experiments, which creates four simulated hearts (one sample imaged from two sides) and four control samples, each containing images from the nine locations. An example of the final images can be seen in figure 2. Most images were 2048x2048 pixels and had a ratio of 4.8177 px/um.

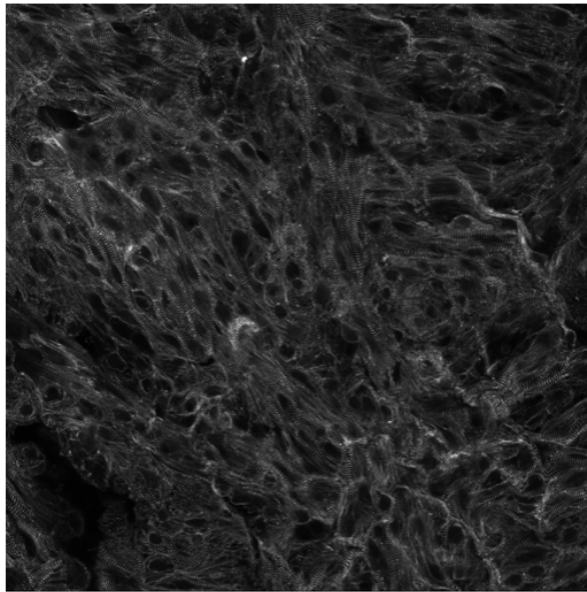


Number	Description
1	Top Left
2	Top Middle
3	Top Right
4	Middle Left
5	Middle Middle
6	Middle Right
7	Bottom Left
8	Bottom Middle
9	Bottom Right

Figure 1: Image orientation of the mini-hearts



Stimulated MH_27



Control MH_28

Figure 2: Example of two images of mini-heart samples, labeled and captured with the Zeiss LSM 880 confocal microscope. The left image is of a simulated sample, and the right is of a control sample. Both images are from the middle-left orientation.

3.2.4 Z-line segmentation

For two of the image analyzing methods, some preprocessing of the images is required. These methods use the Z-discs as guiding points for calculating different characteristics of the fibrils. To perform the segmentation, we will use a pipeline shown in Figure [3]. This pipeline is implemented in ImageJ [Ima].

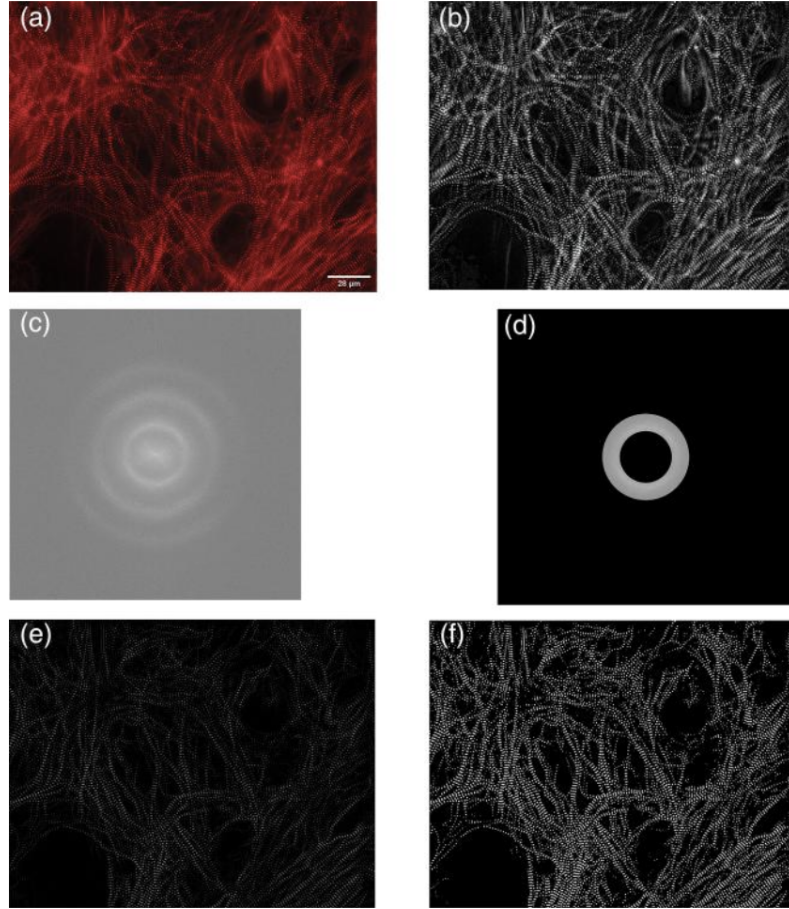


Figure 3: Pipeline for creating the binary mask of the Z-disks form the original images. Image source: [CSD⁺²²]

First, we perform a background subtraction and sharpen the image. Next, a 2D-FFT conversion with a bandpass filter of $1.2\text{--}2.0 \mu m$ is applied. These boundaries were selected because sarcomere lengths are typically $1.6\text{--}1.8 \mu m$ in hiPSC-CMs and up to $2.2 \mu m$ in mature human adult CMs [CSD⁺²²]. The average sarcomere length is set at $1.6 \mu m$, and the bandpass filter range of $1.2\text{--}2.0 \mu m$. This ensures removal of noise while segmenting the Z-lines within these boundaries. The conversion of the bandpass filter to a frequency domain is calculated using the image dimensions, the pixel-to-micrometer ratio, and a formula to determine the frequency boundaries [Eff00]. The frequency domain shows the frequency of patterns which we can use to single out the sarcomere pattern.

$$Frequency = \frac{N}{(R * SL)} \quad (1)$$

N: Closest power of two relative to the maximum width or height of the image

R: Pixel-to-micrometer ratio

S: Upper frequency bound

L: Lower frequency bound

Using this formula [1], the upper and lower frequency bounds are calculated, defining the boundaries in the frequency domain. All data outside these bounds is removed. Subsequently, a reverse FFT operation is applied to restore the image, retaining only the signals within the specified frequency band. Finally, a hard threshold is applied to filter out trivial signals, resulting in a binary mask of the original image. This binary mask can then be used in the methods for further analysis.

4 Experiments

To analyze fibril maturation in 3D organoid samples, three different existing methods were used. The input data is created by the university of Twente and the full protocol will be discussed. The methods were adjusted to the new input data and integrated into a Tool. With the results we will analyze the performance of the different methods and discuss the cardiomyocyte maturation.

4.1 Fibril analysis

The first algorithm was created by PhD candidate Linde Schoenmaker in 2021 and retrieves a full analysis of the fibril structures [CSD⁺²²]. It identifies fibrils in each image and calculates different metrics. This approach relies on the Z-disks as a guide for the fibrils and therefore requires a binary mask as input. In section 3.2.4 an explanation is provided on how to retrieve the binary mask from an original image. In figure 5, you can see the flowchart of the full process. First, the image is skeletonized using the skeletonization function of Sci-Img [Sci]. The Z-disks are then identified and established in a coordinate system. The method accounts for crowded regions and retrieves the Z-disk centroids and orientations. Using this as a base, the myofibrils are traced. A recursive function finds neighbors and tracks unassigned Z-disks. Here, myofibrils are built recursively until all Z-disks are assigned. Finally, fibrils are connected until all are assigned.

The algorithm also includes the option to generate an image where the fibrils are traced in different colors and overlaid on the original images. In image 4, there is a visual representation showing the skeletonized image and the final image with traced fibrils.

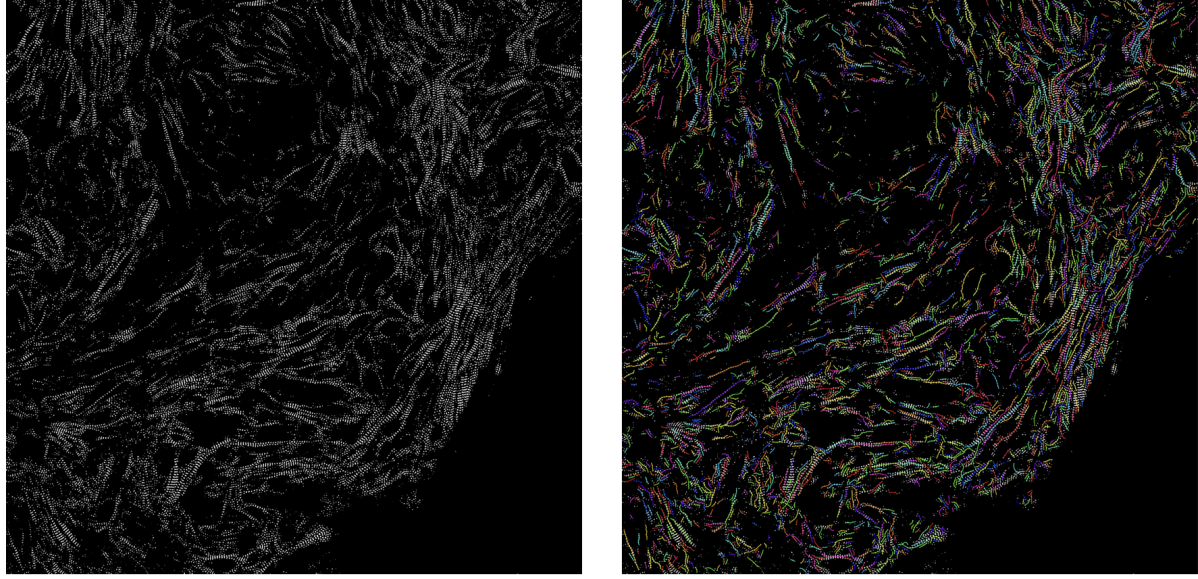


Figure 4: Visual representation of the fibril tracing done by the algorithm. First image shows a binary mask of a sample. Right image shows the fibril tracing

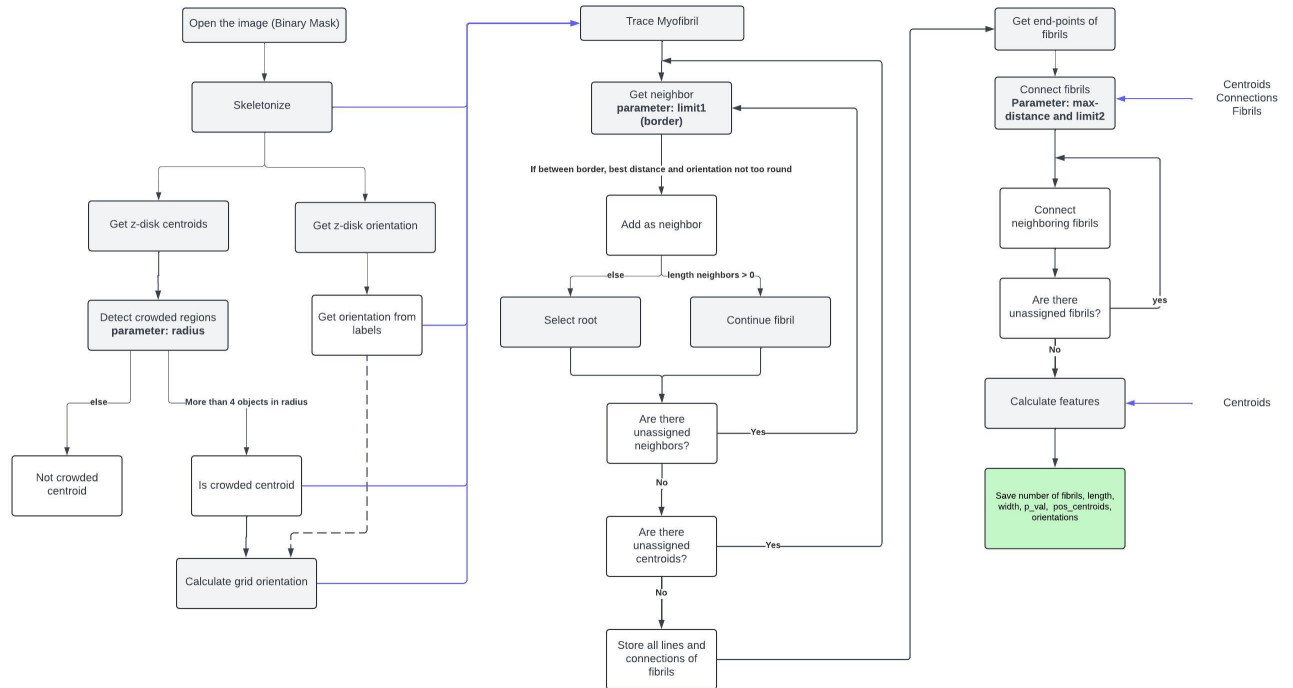


Figure 5: Pipeline for identifying fibrils and calculating its metrics.

With the completed fibrils, the following features are calculated:

- Number of found fibrils.
- Average length and width of fibrils with standard deviation.
- Organized orientation, as the p-value of a Chi-Square test on orientation distribution.
- Percentage assigned, calculated as the ratio of total centroids to connected centroids.
- Orientation frequency of the fibrils, divided into four directions (\backslash , $/$, $-$, $|$).

The original code required some modifications. Since the algorithm was only suitable for images with a ratio of 5.6, adjustments were made to ensure the algorithm could accommodate different image ratios. The main task was to identify the parameters that are affected by ratio changes and make them adjustable. A list of the adjustable parameters is shown in table 1. Additionally, some structural elements had to be modified to accommodate the tool, but these changes did not significantly alter the algorithm.

4.2 Sarcomere Analysis

The other two methods analyze the sarcomere structure. Sarcomeres are contractile units, which makes the measurements challenging. As discussed earlier, sarcomeres are the repeating structures of myofibrils, making them a good focal point for researching fibrils. We will use the Z-disks (orthogonal filaments of the sarcomere) as a guiding point to study the sarcomeres. Two different methods will be presented. The code for both of these methods was created by Tijmen van Wel in 2023 [vW23].

4.2.1 BM tracing

The first method uses a coordinate system from the binary mask of an original image. The image is then first skeletonized. A double loop is used to find edge-points of the Z-lines in the skeleton. With a recursive function the other edge-point is then found. For each of the coordinate pairs the length and angle is calculated. Next, the program checks whether lines are neighboring Z-lines. Tijmen used edge points for his calculations instead of middle points to avoid skewed results [vW23]. Since edge based calculations give both shorter and longer lengths it ensures a balanced average [vW23]. Finally all the distances are averaged and divided by the image pixel to μm ratio. The full pipeline can be seen in image 7. This method also creates a visual presentation of the found sarcomere structures, which you can see in image 6. Once the tracing is done the following metrics are returned:

- Average sarcomere length.
- Total amount of traced Z-disks.
- Total amount of created lines between Z-disks (amount of sarcomere structures that are traced).
- Ratio between number of Z-lines and connected lines.

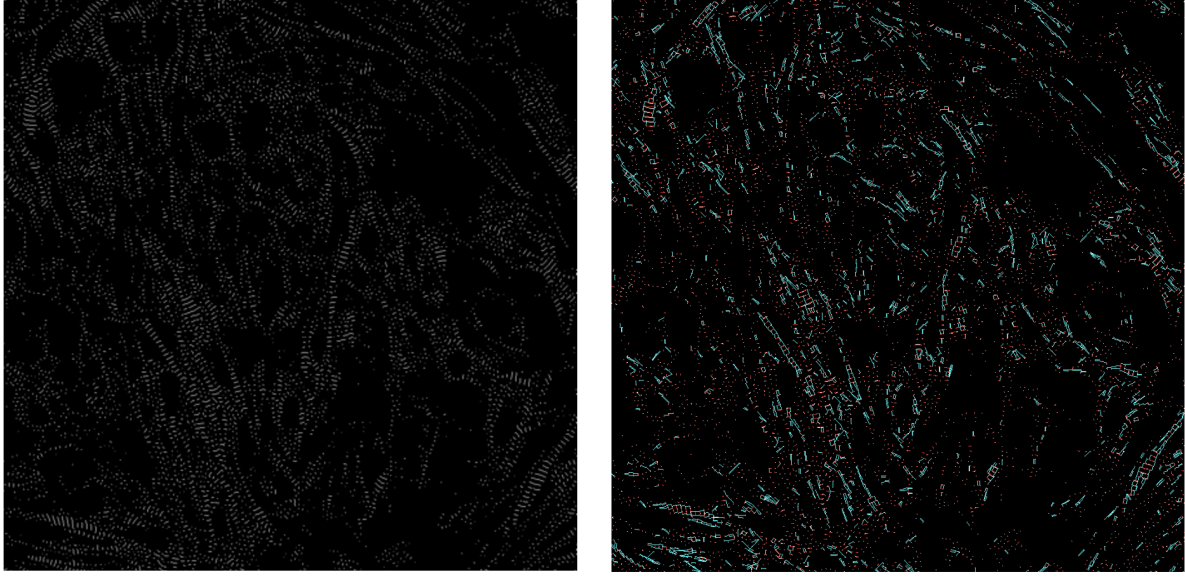


Figure 6: Visual representation of the sarcomere tracing performed by the algorithm. The first image shows a binary mask an original image with skeletonization. The right image displays the Z-disk tracing (in red) and the sarcomere structures (in blue).

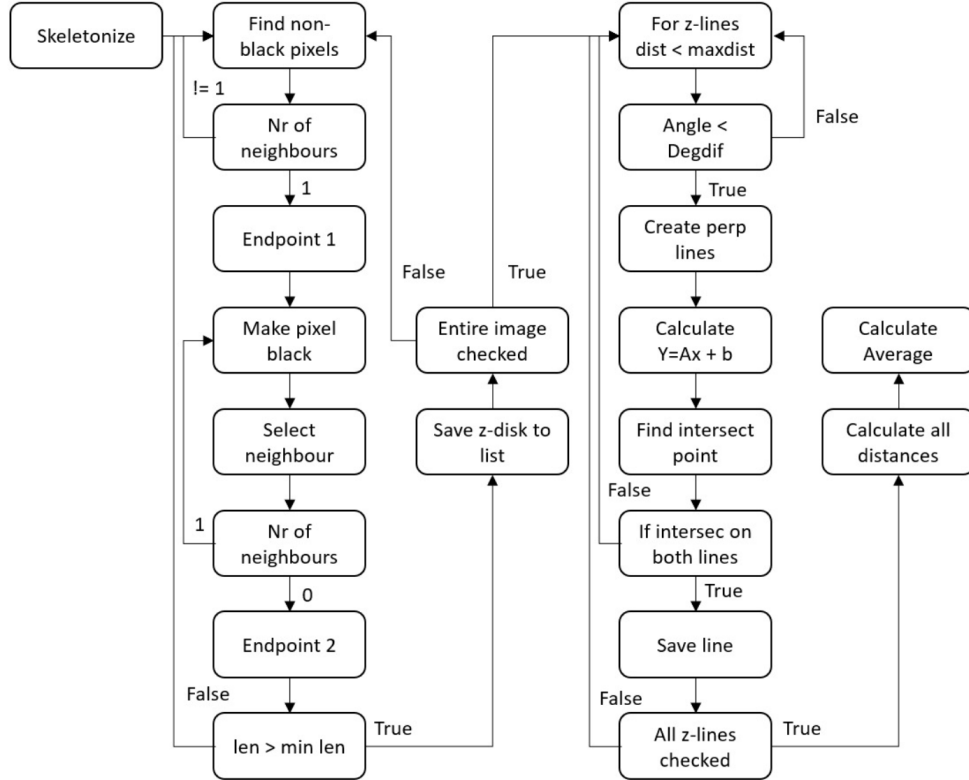


Figure 7: Pipeline for the sarcomere tracing from binary mask. Image source: [vW23]

4.2.2 FFT-2D

The last algorithm is based on a commonly used method for calculating sarcomere lengths [PKV12] [IEC10]. The code for this method was also created by Tijmen van Wel in 2023, a full pipeline of his code is seen in image 10.

The FFT method uses the 2D-FFT conversion of the original image. In the original image, each pixel represents a specific brightness or intensity, reflecting spatial information. The 2D-FFT converts this spatial information into the frequency domain, where each pixel in the transformed image corresponds to a frequency component (see image 8). Bright spots indicate repeating patterns, such as sarcomere spacing. Therefore, this algorithm uses a 2D-FFT converted image from the original as input, instead of the binary mask used by the other methods. This process is also performed manually using ImageJ [Ima].

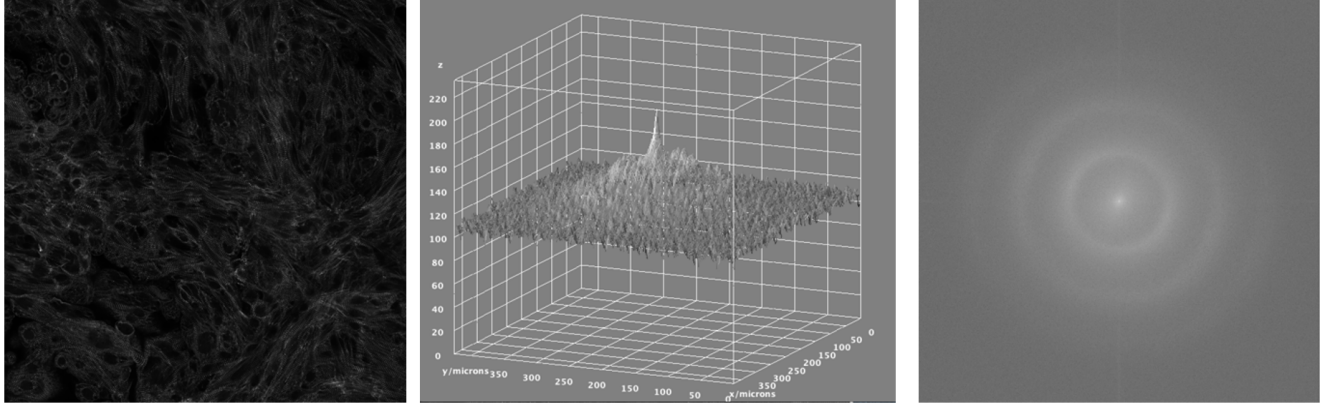


Figure 8: Visual representation of the 2D-FFT transformation of an image. The first image is an original control heart image. The second image shows the 3D frequency domain of the spatial information. The right image is a 2D conversion of the 3D representation.

To reduce noise, we set frequency bounds based on typical sarcomere lengths, ensuring we focus on meaningful frequencies (as seen in image 9). The boundaries are calculated based on the image properties with formula 1. This approach also helps retrieve the binary masks of Z-disks, as discussed in section 3.2.4. Finally, we calculate the total brightness and the number of pixels at each distance, creating an average brightness distribution. The Fitter module is used to calculate the corresponding normal distribution [Fit]. In Image 9, the peak of this distribution represents the average sarcomere length, which is then converted to micrometers (μm). Once the algorithm is done, only the average sarcomere length is returned.

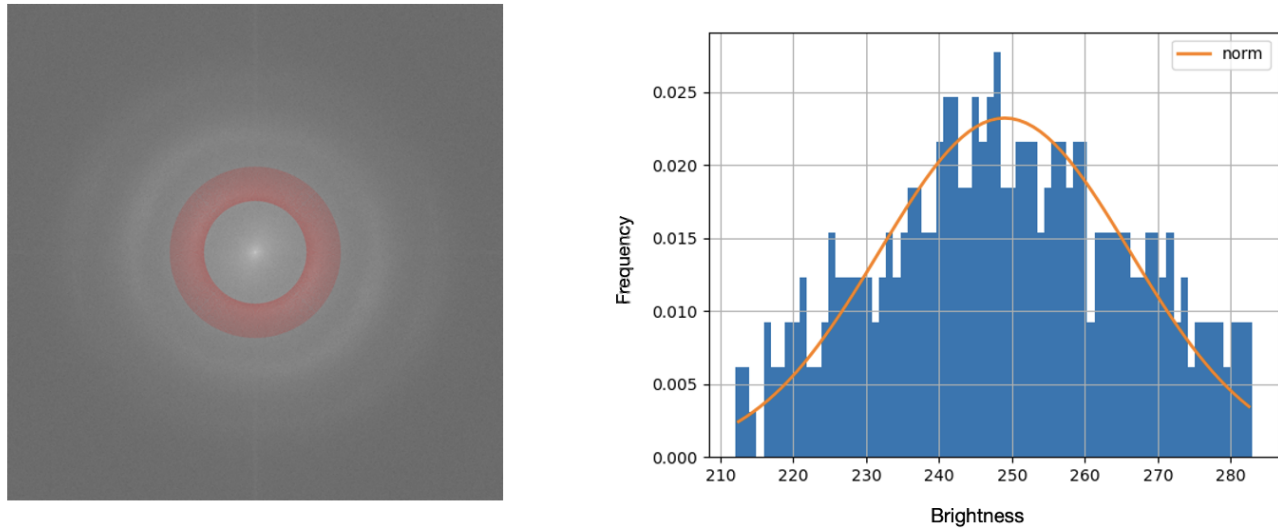


Figure 9: Right images shows the 2D-FFT with the frequency bound (red space). Left image shows the brightness distribution within the frequency bound. The peak represents the average sarcomere length before converging back to micrometers

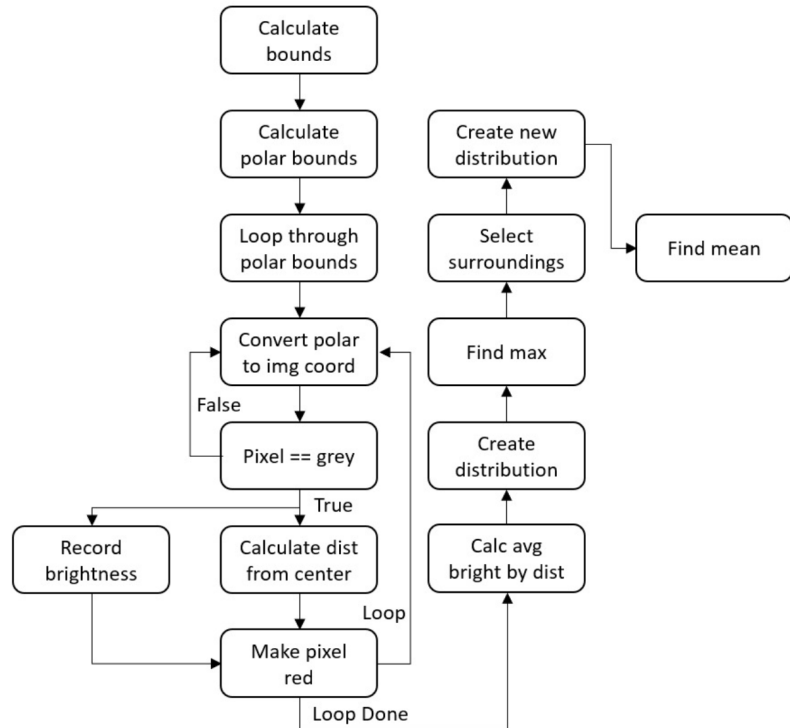


Figure 10: Pipeline for creating the binary mask of the Z-disks form the original images. Image source: [CSD⁺22]

4.3 The tool

The above algorithms were developed by different individuals, each of whom designed methods for slightly different images. Therefore, each algorithm had to be adjusted to fit the new input. For example, the original samples were created under 2D culturing conditions. The new images contained more noise and a higher fibril density due to the 3D culturing conditions. Moreover, the new images had a different pixel to micrometer ratio and size. It was also important that the methods would be accessible to biologists who could use them easily without requiring knowledge of informatics. Therefore, a tool was created that encompasses all the methods. The algorithms were implemented in Python, and the Tkinter package was used to create a basic interface [tki].

4.3.1 Parameters

To make the algorithms more accessible for slightly varying input images, parameters were extracted from the code and made adjustable in the user interface. Each algorithm has its own set of parameters that influence the analysis method. For the images used in this research, the parameters were visually adjusted as needed by visually examining the output images. These values were also set as the default settings. A list of all the adjustable parameters for each algorithm is shown in the tables 1 2 3.

Parameter	Default Value	Type	Description
Ratio (px/um)	4.8177	float	Ratio of the image in pixels per micrometer.
Radius (px)	14	integer	Threshold for determining if a region is crowded (4 objects within the radius).
Max_distance (px)	14	integer	Maximum distance between Z-disks used to establish connections.
Limit border (px)	16	integer	Limit for Z-disks near the image border.
Limit endpoints (px)	20	integer	Maximum distance allowed between endpoints of Z-disks.

Table 1: Fibril analysis parameters, with their default value.

Parameter	Default Value	Type	Description
Ratio (px/ μ m - float)	4.8177	float	Ratio of the image in pixels per micrometer (px/ μ m).
min.length_skeleton (μ m - float)	0.5	float	Minimum length a Z-disk skeleton must have.
list_width (integer)	100000	integer	Bound within which points are checked when maintaining a list.
deg_dif (px - integer)	20	integer	Maximum distance between lines to ensure they are not too far apart.
check_distance (px - integer)	13	integer	Maximum distance between Z-line couples.

Table 2: Sarcomere analysis tracing parameters, with their default value.

Parameter	Default Value	Type	Description
Ratio (px/ μm - float)	4.8177	float	Ratio of the image in pixels per micrometer (px/ μm).
upper_s_len (μm - float)	2.0	float	Maximum sarcomere length.
lower_s_len (μm - float)	1.2	float	Minimum sarcomere length.
full_coverage (True or False)	False	bool	Whether all pixels in the bandpass are checked.
lines_from_center (degrees - integer)	360	integer	Number of degrees in the circle that are checked.
interval_coverage (float)	0.0004	float	Number of intervals in the circle checked; the value is multiplied by π .

Table 3: Sarcomere analysis FFT parameters, with their default value.

4.4 Results

For each of the samples, nine images are taken from different orientations (see image 1). Therefore, each sample has nine images to analyze, and feature calculations are performed for each orientation. The results will be averaged over the nine orientations. We do not analyze each orientation separately or look at differences within samples.

4.4.1 Fibril Analysis

First, we will take a look at the results from the fibril analysis method. This method calculates a number of features. In Figure 11, we can see the different feature calculations of the analyzed samples. When we examine the total number of fibrils in Figure 11a, there is quite some variation between the control and stimulated samples. However, with the exception of the group MH25 and MH26, it appears that the stimulated samples tend to have a higher fibril count on average. This trend is seen when looking at the average fibril length in Figure 11b. Again, with the exception of MH26, there is a clear difference in lengths, where the stimulated samples show a greater length. When examining the average fibril width 11c, we observe that the control group tends to have a higher width on average. However, this time, groups MH21 and MH5 show a significant difference, with the stimulated group having an higher average for fibril width.

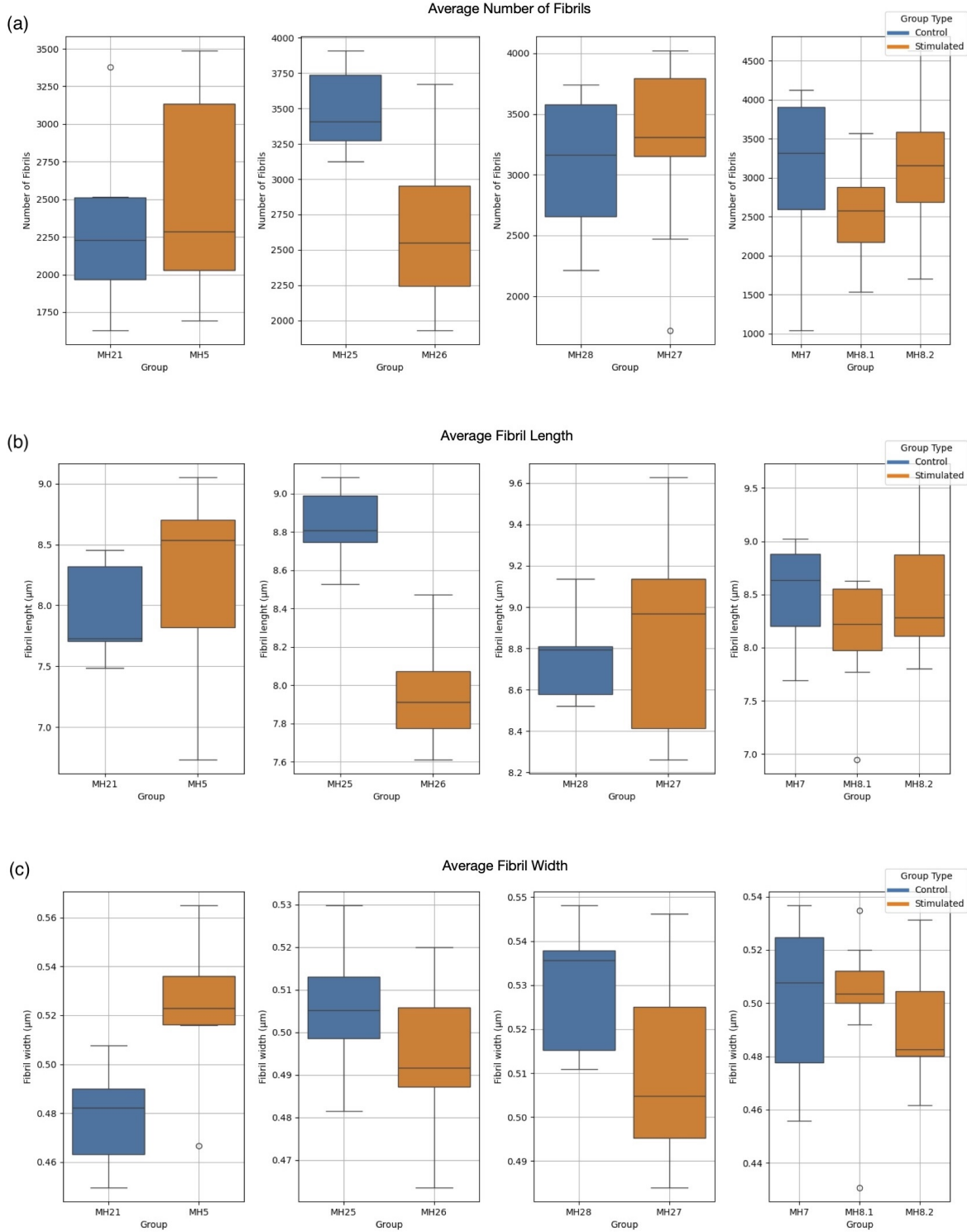


Figure 11: Results from Fibril analysis of the different samples. Summarizes the (a) average number of fibril, (b) average length and (c) average width. Graphs are grouped based on the sample pairs (stimulated and control). Blue represents the control samples and orange the stimulated samples.

We can also examine the average orientation distribution of the analyzed fibrils. In Figure 12, the average fibril orientation for each sample group is shown, with the different x-axis labels representing the different directions. There seems to be a lot of variation within the groups, with some groups showing clearer differences than others. Most notably, MH21 and MH5 stand out. MH21 (control) shows a higher frequency for the diagonal orientation, while MH5 does not show a spike for any particular orientation. For MH7 and MH8, the stimulated group shows more aligned results than the control group. The other groups show similar distributions between the pairs.

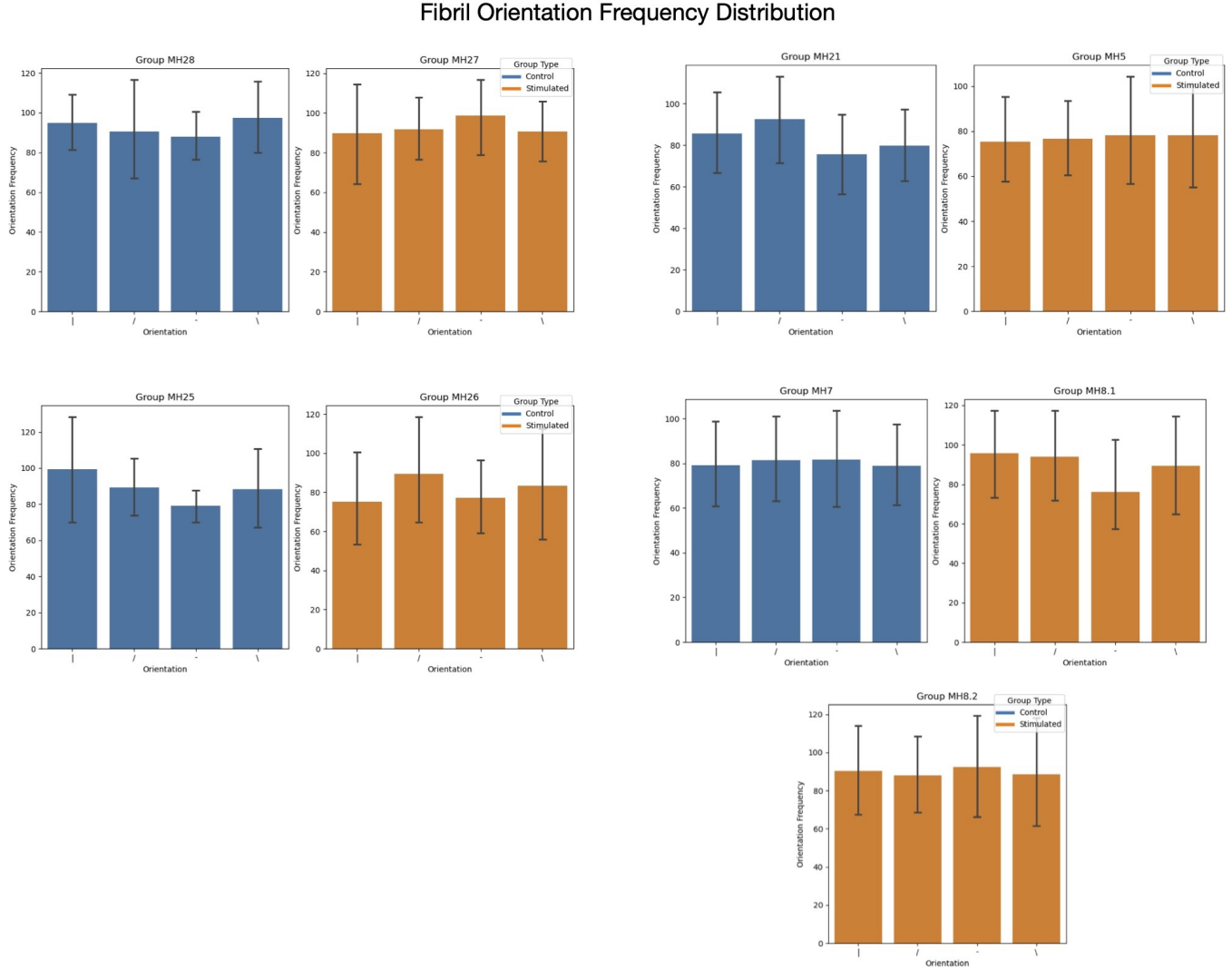


Figure 12: Orientation distribution from fibril analysis. For each sample the average fibril orientation is summarized. Graphs are grouped based on the sample pairs (stimulated is orange and control is blue). Where — represents vertical, / and \ diagonal, and - horizontal.

4.4.2 Sarcomere Analysis

The two other methods, FFT-2D and BM Tracing, both analyzed the average sarcomere length. First, we examine the FFT method. In this method, the images were transformed into a 2D frequency domain. With a bandpass filter the average sarcomere length was retrieved. It is important to note that, upon visually analyzing the transformed images and their brightness distribution, not all images showed a clear peak. An example can be seen in figure 13. This will be further discussed in the discussion section. When reviewing the final data from the FFT method in Figure 14, we observe that, on average, the sarcomere length of stimulated samples is greater than that of their corresponding control samples. Again, group MH26 consistently demonstrates smaller sizes compared to its control group.

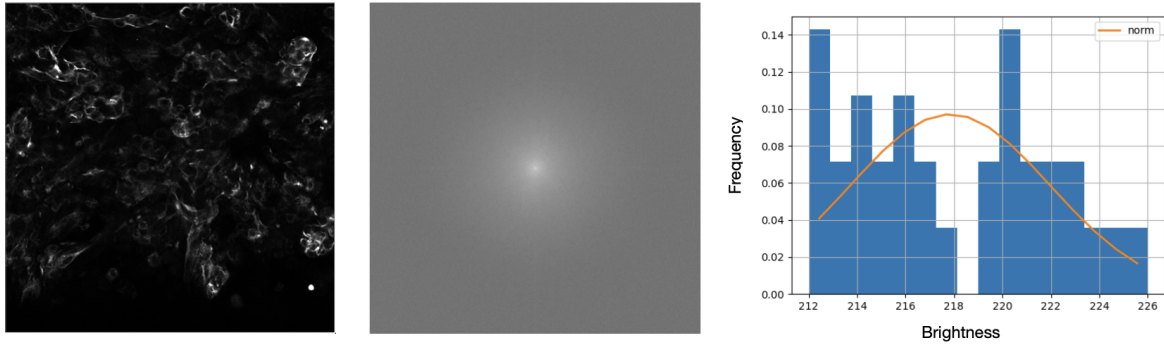


Figure 13: Image transformation of sample MH8.1 from the bottom center orientation. Frequency distribution shows no clear peak in brightness.

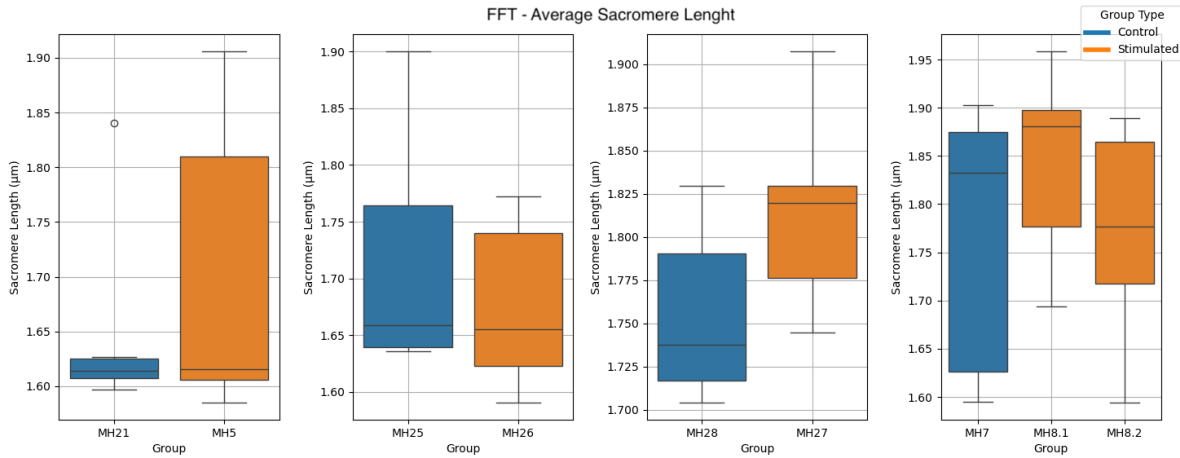


Figure 14: Results from the FFT-2D analysis. The graphs show the average sarcomere length per sample pairs (stimulated: orange and control: blue).

Next, in Figure 15, the average sarcomere length from the Binary Mask Tracing method is presented. This method uses the binary mask of Z-disk to trace sarcomere structures. Here, we do not observe a clear distinction between the stimulated and control pairs. However, in some cases (MH28 and MH27, MH7 and MH8), there is greater variability in sarcomere length within the control groups.

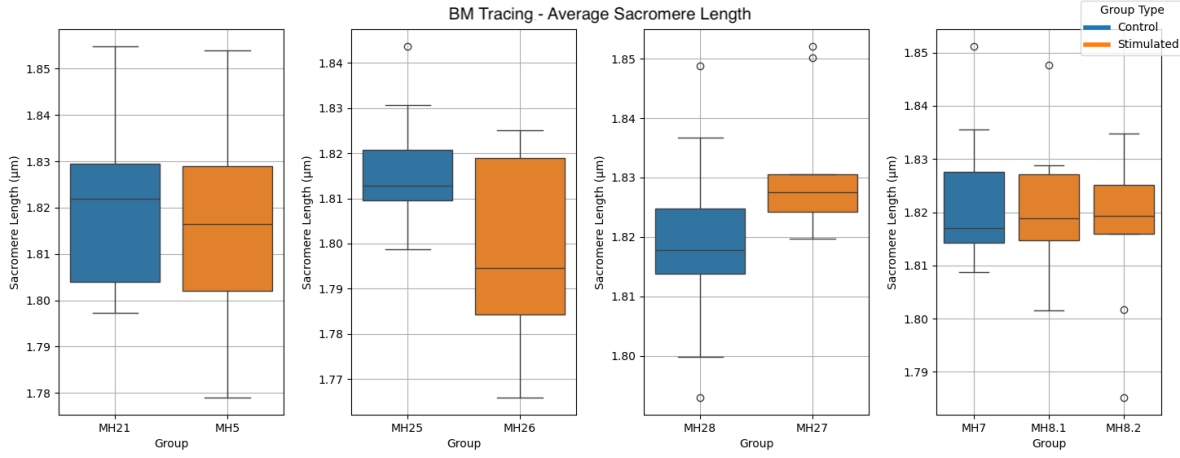


Figure 15: Results from the BM tracing analysis. The graphs shows the average sarcomere length per sample pairs (stimulated: orange and control: blue)

4.4.3 Runtime

The average runtime for each method is shown in table 4. The runtime is averaged over all samples and shows how long each method takes to analysis 9 images. We can clearly see that the 2D-FFT method has a significant fast runtime compared to the other methods. BM tracing does lie furthest from the other methods and taken over ten minutes to process 9 images.

Method	Average Runtime (seconds)	Amount of Images Processed
Fibril method	63	9
BM tracing	786	9
2D-FFT	2.6	9

Table 4: Method performance comparison

5 Conclusions and Further Research

The results show several interesting findings. First, one of the most noticeable observations is the comparison between the MH25 control and MH26 stimulated pairs. In most metrics, the control group consistently shows higher results, suggesting more maturation. The only exception is in the orientation distribution, where the stimulated group appears to have slightly more central

alignment. To gain further insights, the images of the MH26 and MH25 samples were visually analyzed. The images of the control group did show less noise and more clear fibril structures. The MH26 sample shows a lot of black circular structures and more noise compared to the MH25 sample (see image 16). Whether these results were due to experimental errors or if the control group truly exhibited better maturation is uncertain. Since these are 3D organoid samples, the tissues had to be somewhat flattened which could influence the image quality. Overall, we will consider this abnormality when discussing the overall results.

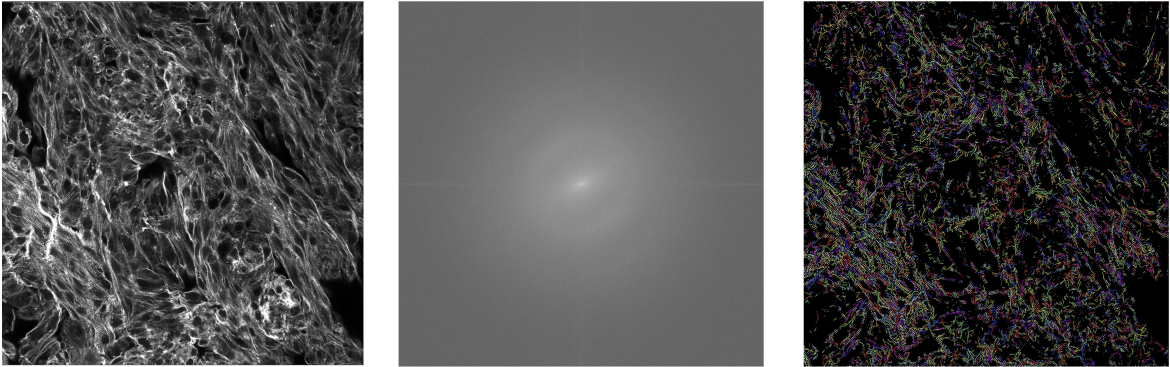


Figure 16: Example image from MH26 (stimulated) from the bottom left orientation, with the 2D-FFT conversion and the fibril tracing. Image shows a lot of noise and unorganized structures.

Second, when considering the runtime of the algorithms, it is clear that the FFT method offers a significant advantage in processing time. The fibril analysis also demonstrated a quick analysis, needing about one minute to process nine images. Given the many different metrics it calculates, this runtime is somewhat valid in comparison to the FFT method. Only the BM tracing method showed a significantly longer runtime, making it less attractive for large datasets. The BM tracing method checks all pixels in the images, which accounts for the longer runtime. The previous work by Tijmen van Wel, who developed the code for these methods, also concluded that the FFT conversion is a favorable method for high throughput image analysis [vW23].

When examining the overall fibril maturation in the control and stimulated pairs, there are signs of slightly improved maturation. Earlier, we discussed that fibril and sarcomere size and alignment are key indicators for determining myofibril maturation. In the following sections, we will delve deeper into the fibril and sarcomere analysis.

5.1 Fibril Maturation

In the fibril analysis method, most pairs showed key differences between stimulated and control samples. On average, stimulated samples showed higher fibril counts and lengths. Cardiomyocyte maturation is defined by myofibril expansion and alignment [GP20]. Therefore, a higher fibril count and average length can indicate a higher level of maturation. However, the average fibril width did not show an increase in the stimulated groups. Mature cardiac fibers tend to be wider, which is important for their functionalities [ATY⁺17]. Thus, we would expect the average width in the

stimulated groups to be higher. However, the stimulated groups consistently exhibited smaller widths. On average, the difference in width between pairs was under $0.2 \mu\text{m}$.

Since the samples are still in early developmental stages, it is possible that the maturation of fibril width is also in its early stage. If more images of samples during the maturation process were available, we could better track changes in fibrils over time, providing additional information. However, the smaller widths, might also suggest that mechanical stimulation primarily enhances fibril alignment and elongation rather than increasing fibril width. To further analyze this phenomenon, a more in-depth research over additional days would be useful.

When examining fibril alignment in sample pairs, there is quite some variation between pairs. Some pairs show better alignment in the stimulated groups, while others exhibit better alignment in the control groups. For example, groups such as MH7 and MH8 demonstrated greater alignment in the stimulated samples. Similarly, as observed in the analysis of fibril width, these results could be caused by similar factors. The variation may reflect experimental limitations, or it may be too early in the development process to observe significant alignment at this stage. Additionally, it is important to note that the samples were placed between two pieces of glass, and some pressure was applied to capture the images. This process could also affect the observed orientation of the fibrils.

5.2 Sarcomere Maturation

Both FFT-2D and BM Tracing methods were used to analyze sarcomere lengths. The FFT showed consistently that the stimulated samples had longer sarcomeres. With the exception of the MH26/MH25 pair, which we discussed earlier and will weigh less in the analysis. The BM method showed more similarity between the stimulated and control groups. With all groups, it could be suggested that the stimulated group had slightly longer sarcomeres (excluding the MH26/MH25 pair). However, this difference is far less significant compared to the results from the FFT method.

Tijmen also discussed these two methods in his paper [vW23]. His images were smaller in size and less complex, with less fibrils and lower densities. He suggested that the BM method calculates actual visible distances, making outliers more impactful on the averages. This can be problematic for images with a low z-disk count but also for those with a high density of Z-disks. Noise and complex structures can go against the method's validity in high-density images. On the other hand, the FFT method has already been shown to be successful in analyzing grown cardiomyocytes, resulting in more validity [vW23]. The FFT method does have issues with low-data images where no clear peak is observed in the 2D-FFT conversion image (such as in the MH26/MH25 sample). However, with higher Z-disk counts, the FFT method does seem to perform better and quickly [vW23]. Therefore, the results from the FFT method hold some greater reliability. With this in mind, it can be concluded that cyclic stretch likely improves sarcomere structure and overall cardiomyocyte maturity.

5.3 Research Conclusion

If we look back at the research questions, we can now discuss the answers. First, we will address how we used existing models to analyze 3D organoid cardiomyocytes derived from hiPSC-CMs.

The 3D organoid culture conditions allowed for a natural development process. This also made the samples more complex, since they could grow in multiple dimensions. To create better-quality images, the samples were flattened between two pieces of glass. The images show a higher Z-disk density and noise.

The existing methods were created for samples that had 2D culturing condition, where images were smaller and less complex. Therefore we had to adjust the existing methods to fit the new input. First of all, we retrieved important parameters that have great influence on the calculation methods. The algorithms were for example dependent on image size and ratio. Next these parameters had to be fine tuned by examining the visual results and recalculating the bandwidth. For the final tool, these parameters can be changed and are explained in the UI.

Overall, different methods needed different adjustments. It was therefore important that the final tool came with a manual to further help biologists use the tool themselves. In the manual an in depth explanation is given for each method and also the image preprocessing steps are explained (for example how to create a Binary mask and a 2D-FFT conversion). Now biologists can use their own images that have their own specifications and fine tune the parameters.

The FFT method showed the fastest analysis and better performance for the 3D organoid samples. It was clearly faster and had a higher reliability in high concentrated Z-disk images. The fibril analysis provided a lot of information with a slightly higher time frame. The BM tracing methods showed to be the least useful, due to the long processing time and lack of validity in crowded Z-disk images.

Next, we look at the effects of multi-axial cyclic preload on mini-heart cardiomyocyte maturation. The experiment data was created by the University of Twente (led by Mariel Cano-Jorg), who are also researching this matter. With the significance of heart research, multiple experiments have been done with different types of stimulation. These also show improved maturation [MLM⁺14] [ATY⁺17] [TMR⁺11]. The results from this experiment also align with those findings, suggesting that the multiaxial cyclic preload on mini-heart could have a positive effect on cardiomyocytes maturation.

5.4 Further Research

In this experiment, we could only suggest cardiomyocyte maturation due to variability in data and lack of and the lack of clear, significant results. We also did not analyze the method's accuracy by manually processing the images and comparing the results. This variability and uncertainty should be further researched, and shows the need for additional data in the growth process to better track the maturation process. The results in fibril height, width and orientation also underlies the need to further research the maturation process. Moreover, did we only look at the maturation process and not the sample's functionality. Combining these characteristics would be significant for making further conclusions.

The sample images were very crowded which made the analysis more challenging. Improvements to the imaging protocol for 3D organoid samples, could enhance the quality of Z-disks observation. Currently, much of the preprocessing of the images relies on manually calculating bandwidth and visually assessing the images. This should become a standard function integrated into the tool to make the methods more accessible. The observed limitations of the methods (primarily BM tracing) suggest a need for more robust imaging techniques. We need methods that better facilitate the

different characteristics and specifications of input data. The tool currently works within a bounded set of image specifications. With the introduction of deep learning and AI, these methods could be further optimized. Overall, these findings emphasize the need for improved high-throughput image analysis methods in cardiac tissue research (and beyond).

References

- [ATA22] Razan E. Ahmed, Takeshi Tokuyama, and et al Anzai. Sarcomere maturation: function acquisition, molecular mechanism, and interplay with other organelles. *Philosophical Transactions of the Royal Society B Biological Sciences*, 377(1864), 10 2022.
- [ATY⁺17] Oscar J. Abilez, Evangeline Tzatzalos, Huaxiao Yang, Ming-Tao Zhao, Gwanghyun Jung, Alexander M. Zöllner, Malte Tiburcy, Johannes Riegler, Elena Matsa, Praveen Shukla, Yan Zhuge, Tony Chour, Vincent C. Chen, Paul W. Burridge, Ioannis Karakikes, Ellen Kuhl, Daniel Bernstein, Larry A. Couture, Joseph D. Gold, Wolfram H. Zimmermann, and Joseph C. Wu. Passive stretch induces structural and functional maturation of engineered heart muscle as predicted by computational modeling. *Stem Cells*, 36(2):265–277, 11 2017.
- [CJKDASCT] Mariel Cano-Jorge, Chloë Kaal, Simone Dem, ten, and TechMed Centre University of Twente Applied Stem Cell Technologies, Department of Bioengineering Technologies. Training a human mini-heart: Effect of dynamic preload on human-engineered ventricles.
- [CSD⁺22] Lu Cao, Linde Schoenmaker, Simone A. Ten Den, Robert Passier, Verena Schwach, and Fons J. Verbeek. Automated Sarcomere Structure Analysis for Studying Cardiotoxicity in Human Pluripotent Stem Cell-Derived Cardiomyocytes. *Microscopy and Microanalysis*, 29(1):254–264, 12 2022.
- [Eff00] Nick Efford. *Digital Image Processing: A Practical Introduction using Java*. 5 2000.
- [Fit] FITTER documentation — fitter 1.7.1 documentation.
- [GHR⁺21] Francis Grafton, Jaclyn Ho, Sara Ranjbarvaziri, Farshad Farshidfar, Anastasiia Budan, Stephanie Steltzer, Mahnaz Maddah, Kevin E Loewke, Kristina Green, Snahel Patel, Tim Hoey, and Mohammad Ali Mandegar. Deep learning detects cardiotoxicity in a high-content screen with induced pluripotent stem cell-derived cardiomyocytes. *eLife*, 10, 8 2021.
- [GP20] Yuxuan Guo and William T. Pu. Cardiomyocyte maturation. *Circulation Research*, 126(8):1086–1106, 2020.
- [IEC10] Benjamin W. Infantolino, Michael J. Ellis, and John H. Challis. Individual Sarcomere Lengths in Whole Muscle Fibers and Optimal Fiber Length Computation. *The Anatomical Record*, 293(11):1913–1919, 9 2010.

- [Ima] ImageJ.
- [KBK20] Shagun Krishna, Brian Berridge, and Nicole Kleinstreuer. High-Throughput Screening to Identify Chemical Cardiotoxic Potential. *Chemical Research in Toxicology*, 34(2):566–583, 12 2020.
- [KFJ⁺09] Thomas E. Kottke, Dennis A. Faith, Courtney O. Jordan, Nicolaas P. Pronk, Randal J. Thomas, and Simon Capewell. The comparative effectiveness of heart disease prevention and treatment strategies. *American Journal of Preventive Medicine*, 36(1):82–88.e5, 2009.
- [mic] Zeiss LSM 880 Confocal Laser Scanning Microscope.
- [MLM⁺14] Anton Mihic, Jiao Li, Yasuo Miyagi, Mark Gagliardi, Shu-Hong Li, Jean Zu, Richard D. Weisel, Gordon Keller, and Ren-Ke Li. The effect of cyclic stretch on maturation and 3d tissue formation of human embryonic stem cell-derived cardiomyocytes. *Biomaterials*, 35(9):2798–2808, 2014.
- [PA20] Andreas S. Panayides and et al Amini. Ai in medical imaging informatics: Current challenges and future directions. *IEEE Journal of Biomedical and Health Informatics*, 24(7):1837–1857, 2020.
- [PE09] Michael S. Parmacek and Jonathan A. Epstein. Cardiomyocyte renewal. *New England Journal of Medicine*, 361(1):86–88, 7 2009.
- [Pen08] Hanchuan Peng. Bioimage informatics: a new area of engineering biology. *Bioinformatics*, 24(17):1827–1836, 7 2008.
- [Pet10] D.A. Peterson. Confocal microscopy. In Katie Kompoliti and Leo Verhagen Metman, editors, *Encyclopedia of Movement Disorders*, pages 250–252. Academic Press, Oxford, 2010.
- [PKV12] Pearu Peterson, Mari Kalda, and Marko Vendelin. Real-time determination of sarcomere length of a single cardiomyocyte during contraction. *AJP Cell Physiology*, 304(6):C519–C531, 12 2012.
- [SAC⁺21] Soraya Scuderi, Giovanna G Altobelli, Vincenzo Cimini, Gianfilippo Coppola, and Flora M Vaccarino. Cell-to-cell adhesion and neurogenesis in human cortical development: A study comparing 2d monolayers with 3d organoid cultures. *Stem cell reports*, 16(2):264–280, 2021.
- [Sci] scikit-image’s documentation — skimage 0.24.0 documentation.
- [Tab01] Larry A. Taber. Biomechanics of cardiovascular development. *Annual Review of Biomedical Engineering*, 3(Volume 3, 2001):1–25, 2001.
- [tki] tkinter — Python interface to Tcl/Tk.

- [TMR⁺11] Nathaniel L. Tulloch, Veronica Muskheli, Maria V. Razumova, F. Steven Korte, Michael Regnier, Kip D. Hauch, Lil Pabon, Hans Reinecke, and Charles E. Murry. Growth of engineered human myocardium with mechanical loading and vascular coculture. *Circulation Research*, 109(1):47–59, 2011.
- [vW23] Tijmen van Wel. Novel way for the calculation of sarcomere length in human pluripotent stem cell derived cardiomyocytes (Leiden University), 2023.
- [WM05] Elizabeth A. Woodcock and Scot J. Matkovich. Cardiomyocytes structure, function and associated pathologies. *The International Journal of Biochemistry Cell Biology*, 37(9):1746–1751, 2005.